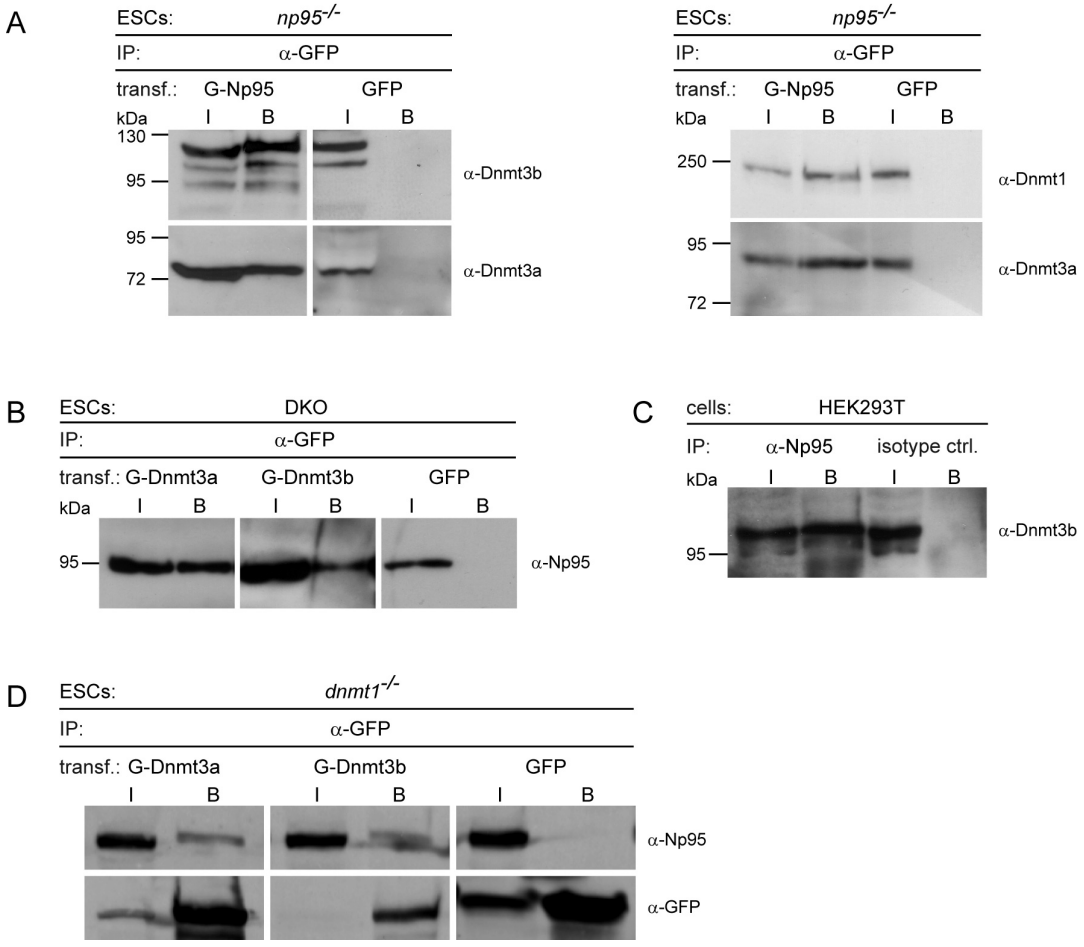

Supplementary Figure S1. Np95 interacts with *de novo* methyltransferases Dnmt3a and 3b. (**A**) Co-immunoprecipitation of endogenous Dnmt3a2 (left and right), Dnmt3b isoforms (left) and Dnmt1 (right) with GFP-Np95 transiently expressed in *np95*$^{-/-}$ ESCs. Left and right panels are from independent experiments where 2 and 4% of input (I) relative to bound (B) fractions was loaded, respectively. (**B**) Co-immunoprecipitation of endogenous Np95 with either GFP-Dnmt3a (left panel) or GFP-Dnmt3b1 (central panel) transiently expressed in DKO ESCs. Transient expression of GFP was used as control (right panel). GFP and GFP fusions were immunoprecipitated with GFP-trap as in experiments shown in Fig. 1B. 2% of input (I) relative to bound (B) fractions was loaded. (**C**) Co-immunoprecipitation of endogenous ICBP90/UHRF1 and DNMT3b in HEK293T cells. Antibodies to mouse proteins cross-react with the respective human homologues. 4% of input (I) relative to bound (B) fractions was loaded. (**D**) Co-immunoprecipitation of endogenous Np95 with either GFP-Dnmt3a or GFP-Dnmt3b1 (lower panel) transiently expressed in *dnmt1*$^{-/-}$ ESCs.

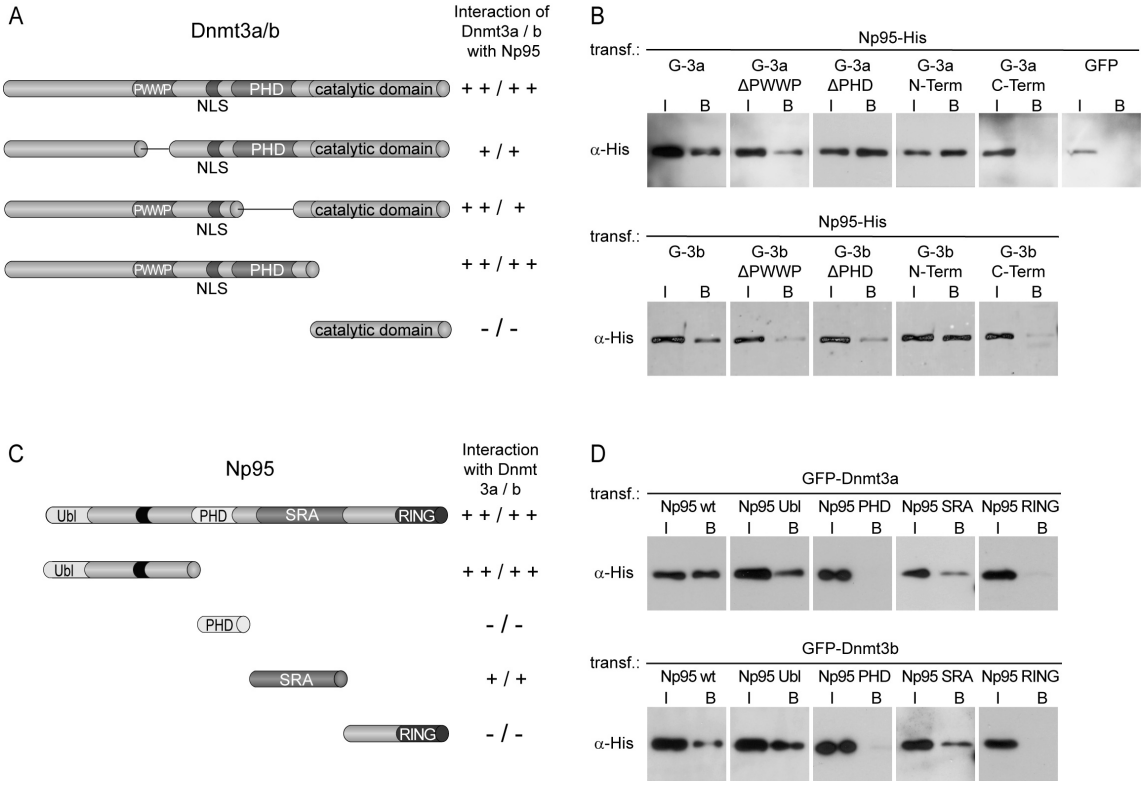

Supplementary Figure S2. Mapping the interaction domains of Dnmt3a/b and Np95. (**A**) Schematic representation of GFP-Dnmt3a/b fusion constructs used for mapping the interaction site with Np95 (N-terminal GFP tag is not shown). (**B**) Co-immunoprecipitation of Np95-His with GFP-Dnmt3 constructs (G-3a/b) from extracts of transiently transfected HEK293T cells. (**C**) Schematic representation of Np95-His constructs used for mapping the interaction site with Dnmt3a/b. (**D**) Co-immunoprecipitation of Np95-His domains shown in c with GFP-Dnmt3a/b constructs from extracts of transiently transfected HEK293T cells. G indicates the GFP fusion. The GFP-trap was used for all the immunoprecipitations in panels B and D. 0.5% of input (I) and 40% of bound (B) fractions were loaded. PWWP, domain with conserved pro-trp-trp-pro motif; NLS, nuclear localization signal; PHD, plant homeodomain; Ubl, ubiquitin-like domain; SRA, set and ring associated domain; RING, really interesting new gene domain. Results of mapping are scored by + or -.

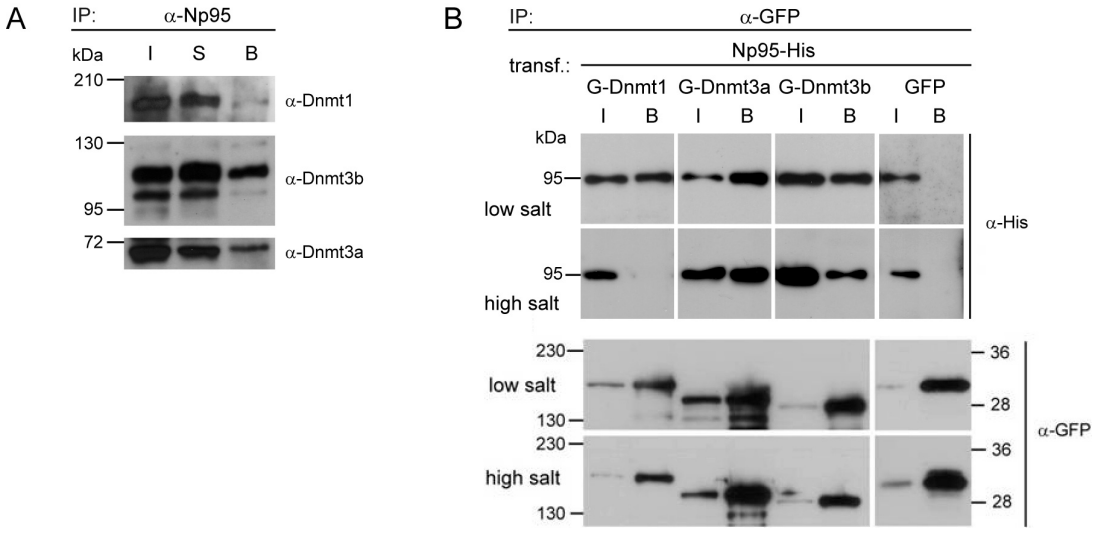

Supplementary Figure S3. Relative stability of Np95 interactions with Dnmt1, 3a and 3b. (**A**) The Dnmt3a/3b blot in Fig. 1A (shown here as middle and lower panels) was reprobed with an anti-Dnmt1 antibody (upper panel) to compare the relative amounts of endogenous Dnmts associated with Np95. The lower panel shows the Dnmt3a2 isoform. (**B**) The blots in Fig. 1C (shown here in the two upper panels) were reprobed with an anti-GFP antibody (two lower panels) to reveal that similar amounts of each GFP construct were immunoprecipitated in low and high salt conditions. Both results point to a tighter association of Np95 with Dnmt3a and 3b as compared to Dnmt1.

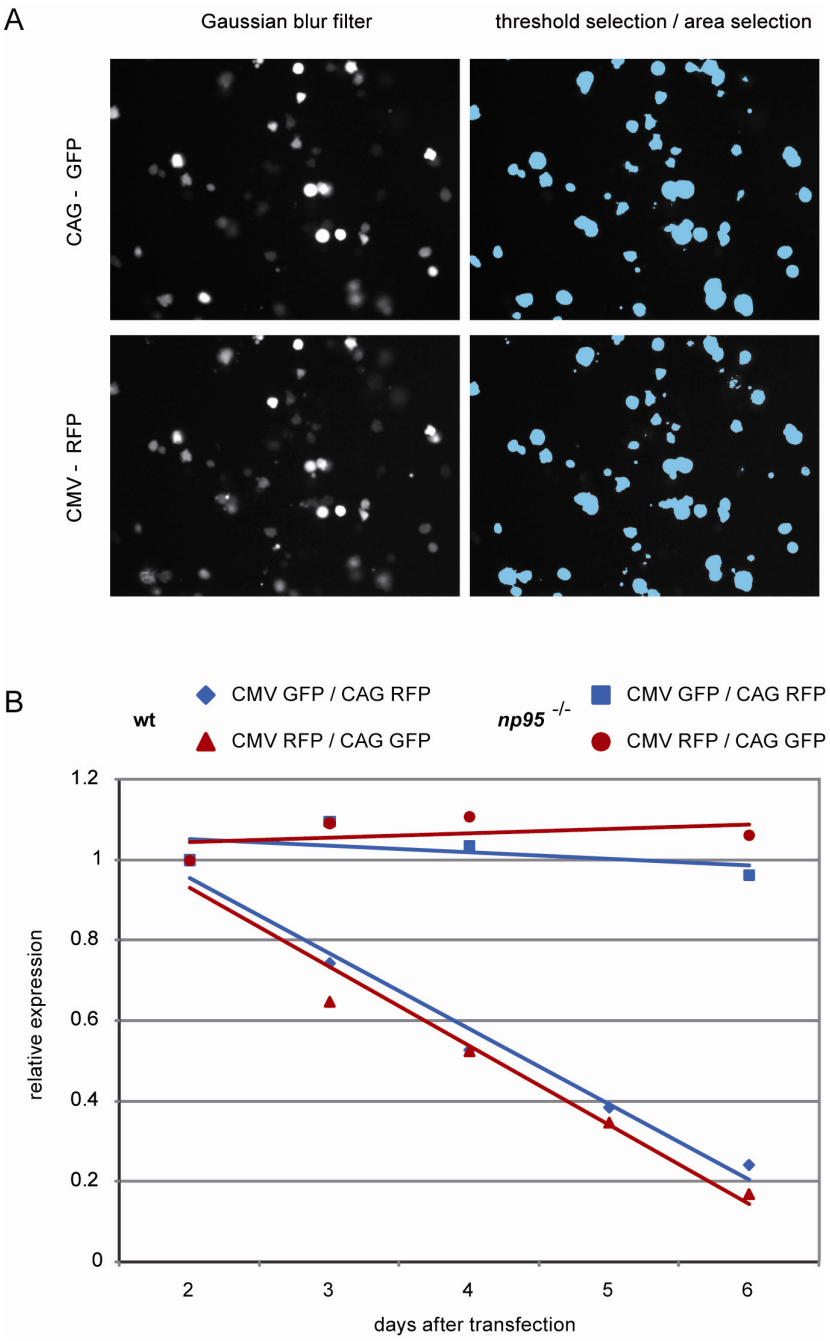

Supplementary Figure S4. (**A**) Automated procedure for quantification of fluorescent signals from digital micrographs for the promoter silencing assay. A macro was written for the ImageJ software that applies a Gaussian blur filter (left panel) and signal thresholding (right panel) to raw images (data not shown) and then calculates the total signal area. (**B**) Silencing assay results are not affected by the choice of fluorescent reporter. wt and *np95*$^{-/-}$ ESC were cotransfected with either CMV-driven mRFP and CAG-driven GFP (red) or CAG-driven mRFP and CMV-driven GFP (blue) expression constructs and the ratio of CMV- over CAG-driven fluorescence was quantified at the indicated time points after transfection as for Figure 2A.

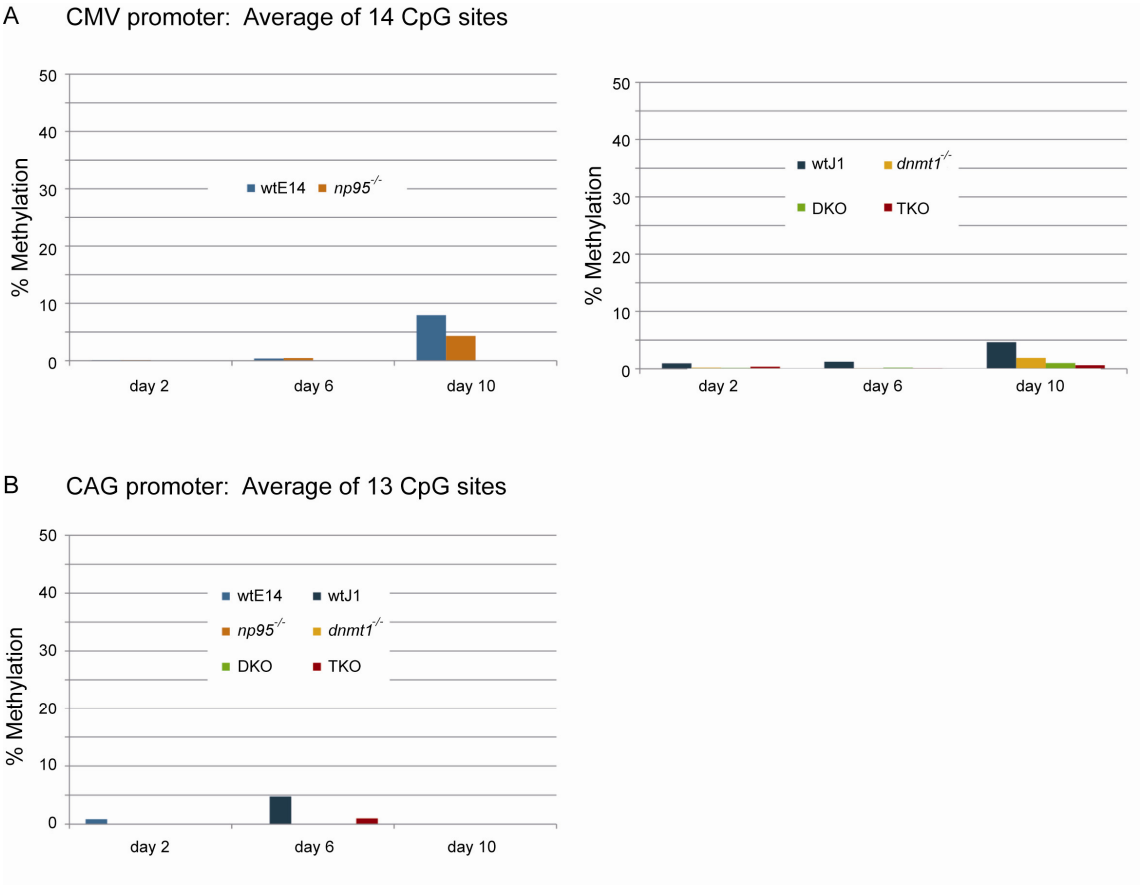

Supplementary Figure S5. Methylation analysis of CMV and CAG promoters 2, 6 and 10 days after transfection. ESCs with the indicated genotypes were transfected, sorted, total DNA was isolated and bisulfite treated as for Fig. 3. **(A)** The same proximal region of the CMV promoter was amplified and pyrosequenced as in Fig. 3. **(B)** A fragment of the CAG construct containing 13 CpG sites was amplified and subjected to pyrosequencing. The analyzed fragment spans across the 3' part of the promoter, the first exon and the 5' part of the first intron of the chicken ß-actin gene and is part of a CpG island. Methylation percentages at individual CpG sites within the respective promoter sequences are averaged. The plot on the left of A was derived from the same data presented in Fig. 3C.

Supplementary methods

Plasmid construction. The CMV-driven enhanced GFP construct was from Clontech (pEGFP-C1). To generate the CMV-driven mRFP construct (pCMV-mRFP) the coding sequence for eGFP in pEGFP-C1 was replaced with that for mRFP from pRSETB-mRFP (Campbell et al, 2002; provided by Roger Tsien). To create CAG-driven eGFP, mRFP and mCherry expression constructs (pCAG-eGFP-IB, pCAG-mRFP-IB and pCAG-mCherry-IB, respectively) sequences coding for the respective fluorescent proteins from pEGFP, pRSETB-mRFP and pRSETB-mCherry (Shaner et al, 2004; also provided by R. Tsien) were inserted downstream to the CAG promoter in the pCAG-IRESblast vector(Chen et al, 2003). The expression construct for Np95-His was described previously (Citterio et al, 2004). To generate expression constructs for GFP-Np95, Ch-Np95, GFP-Dnmt3a and GFP-Dnmt3b1 the sequences coding for Np95, Dnmt3a or Dnmt3b1 were then transferred from the respective CMV promoter-driven constructs (Chen et al, 2003; Citterio et al, 2004) to either pCAG-eGFP-IB or pCAG-mCherry-IB downstream to sequences coding for the fluorescent protein. GFP-Dnmt3a and GFP-Dnmt3b1 deletion constructs were generated by overlap extension mutagenesis(Ho et al, 1989) to remove the following amino acids from Dnmt3a and 3b1, respectively: 278-343 and 223-287 (ΔPWWP); 485-582 and 435-532 (ΔPHD). GFP fusion constructs of N-terminal regions (aa 1-629 and 1-580) and C-terminal domains (aa 630-908 and 581-859) of Dnmt3a and 3b, respectively, were generated by PCR cloning using full length constructs as templates. All constructs were characterised by sequencing and immunoblotting.

Supplementary references

Campbell RE, Tour O, Palmer AE, Steinbach PA, Baird GS, Zacharias DA, Tsien RY (2002) A monomeric red fluorescent protein. Proc Natl Acad Sci U S A 99(12): 7877-7882

Chen T, Ueda Y, Dodge JE, Wang Z, Li E (2003) Establishment and maintenance of genomic methylation patterns in mouse embryonic stem cells by Dnmt3a and Dnmt3b. Mol Cell Biol 23(16): 5594-5605

Citterio E, Papait R, Nicassio F, Vecchi M, Gomiero P, Mantovani R, Di Fiore PP, Bonapace IM (2004) Np95 is a histone-binding protein endowed with ubiquitin ligase activity. Mol Cell Biol 24(6): 2526-2535

Ho SN, Hunt HD, Horton RM, Pullen JK, Pease LR (1989) Site-directed mutagenesis by overlap extension using the polymerase chain reaction. Gene 77(1): 51-59

Shaner NC, Campbell RE, Steinbach PA, Giepmans BNG, Palmer AE, Tsien RY (2004) Improved monomeric red, orange and yellow fluorescent proteins derived from Discosoma sp. red fluorescent protein. Nat Biotechnol 22(12): 1567-1572